



Facile fabrication and catalytic activity of nickel to ferric oxide nanoparticles for ammonium perchlorate decomposition

Sherif Elbasuney^{1,2} · Shukri Ismael² · M. Yehia² · Gharieb S. El-Sayyad³

Received: 26 September 2022 / Revised: 15 December 2022 / Accepted: 2 January 2023 / Published online: 18 January 2023
© The Author(s) under exclusive licence to Associação Brasileira de Engenharia Química 2023

Abstract

Ferric oxide is used in a composite solid propellant as a ballistic modifier, Ni could offer highly catalytic performance compared to ferric oxide due to partially filled d-shell to accept electron and a high magnetism to increase the mobility of the electrons. This study reports on the facile fabrication of nickel and ferric oxide nanocluster of 10 nm, and 5 nm particle sizes, respectively. Fabricated nanocluster were re-dispersed in organic solvent and effectively integrated into ammonium perchlorate (AP). Elemental mapping confirmed uniform nanocluster particle dispersion into AP. The catalytic efficiency of nickel was evaluated to Fe₂O₃ nanocluster using DSC and TGA. AP demonstrated endothermic crystallographic phase change at 242 °C, with subsequent two exothermic decomposition reactions. Nickel demonstrated decrease in endothermic phase change by 49% compared with 39% for ferric oxide; this catalytic action indicate low activation energy. Whereas AP demonstrated total heat release of 742 J/g; nickel offered enhanced heat output by 89% compared with 57% for ferric oxide. The two main decomposition peaks were merged into single peak. Nickel nanocatalyst demonstrated decrease in AP activation energy by – 10% and – 12% using Kissinger and KAS models, respectively. This manuscript shaded the light on nickel as novel emergent nanocatalyst with superior performance for advanced energetic systems.

Keywords Catalyzed propellant · Oxidizer · Ammonium perchlorate · Thermal behavior

Introduction

Ammonium perchlorates (AP), with active oxygen content (34%), is the most frequent oxidizer in highly energetic materials like propellants, explosives and pyrotechnics. (Conkling and Mocella 2012, Elbasuney et al. 2019, Elbasuney et al. 2020). AP could decompose with the release of free oxygen. AP exposes complex decomposition process with phase transition from an orthorhombic to a cubic

structure at 240 °C; this strong endothermic crystallographic phase change could withstand high activation energy (Dillier et al. 2020, Figueiredo and Brójo 2017, Jain et al. 2019, Manash and Kumar 2019, Meyer et al. 2007, Pang et al. 2020, Tang et al. 2020). AP crystal lattice becomes unstable and melts at 557 °C; therefore AP undergoes degradation along with dissociative sublimation Below 100 K/min (Cai et al. 2008). While degradation reaction accounts for 70 wt%; endothermic dissociative sublimation accounts for 30 wt%. Dissociative sublimation results in the evolution of ammonia (NH₃) and per-chloric acid (HClO₄); ammonia-perchloric acid expose luminous bluish flame with temperature up to 1300 K (See Fig. 1) (Arroyo et al. 2020; Dubey et al. 2013, Ishitha and Ramakrishna 2014, Sharma et al. 2015).

Combustion reactive species undergo a sequence of chain reactions to form a premixed flame with final products i.e. O₂, NO, and N₂O. It is considered that the AP deflagration in the gas phase is a surface phenomenon that occurs concurrently with the condensed-phase breakdown. As a result, in the current model, the condensed phase also has a shallow reaction layer and a warmed zone (which includes the melt layer and the AP deflagration zone). However the strong

✉ Sherif Elbasuney
s.elbasuney@mtc.edu.eg; sherif_basuney2000@yahoo.com

✉ Gharieb S. El-Sayyad
Gharieb.Elsayyad@gu.edu.eg;
Gharieb.Elsayyad2017@gmail.com

¹ Head of Nanotechnology Research Center, Military Technical College (MTC), Cairo, Egypt

² School of Chemical Engineering, Military Technical College (MTC), Cairo, Egypt

³ Department of Microbiology and Immunology, Faculty of Pharmacy, Galala University, New Galala City, Suez, Egypt

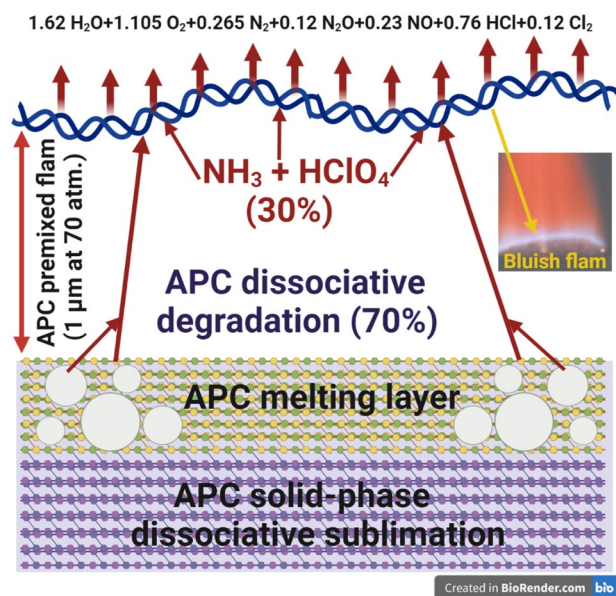


Fig. 1 Schematic for ammonium perchlorate combustion wave structure Adopted from Ref. (Cai et al. 2008)

endothermic crystallographic phase as well as endothermic sublimation process could withstand high activation energy; such endothermic processes could render high burning rate regimes (Dillier et al. 2020; Tang et al. 2020). Catalyzed combustion process can secure low activation energy; consequently stable burning at high reaction rate could be accomplished (Budhwar et al. 2018; Sangtyani et al. 2019).

Recently much research was directed to nanocatalysts which have the potential to enhance AP decomposition (Elbasuney and El-Sayyad 2020, Elbasuney and Yehia 2019, 2020). In more details, Gaete et al. (2022) synthesized the magnetite NPs (Fe_3O_4 NPs) and were functionalized with two different amine derivative groups, tertiary amine and quaternary amine. After that, they were investigate their role in the thermal decomposition of AP. Additionally, Wang et al. (2005) synthesized NiO NPs by solid-state reaction and studying their catalytic activity in the thermal decomposition of AP. The results indicating that, adding 2% of NiO NPs to AP decreases the decomposition temperature by 93 °C and increases the heat of decomposition from 590 to 1490 J g^{-1} . Finally, Zheng et al. (2014) conduct $\text{Cu}(\text{OH})_2 \cdot 2\text{Cr}(\text{OH})_3$ NPs and its accelerating effect and mechanism on thermal decomposition of AP were investigated. The electron transfer process plays a major role in the decrease of the onset temperature of AP decomposition, while the nano-effect is beneficial to easier enrichment of Cu ions on the surface of $\text{Cu}(\text{OH})_2 \cdot 2\text{Cr}(\text{OH})_3$ NPs (Zheng et al. 2014).

Certain metal oxides (i.e. ferric oxide) can catalyze AP decomposition offering low activation energy (Elbasuney and Yehia 2019). However transition metal particles can

secure entirely different catalytic properties (Elbasuney 2018; Elbasuney et al. 2018). Transition metals with partially filled d-shell electrons can experience: variable oxidation state, co-ordination and multifunction capability, and exothermic combustion (Yadav et al. 2020). Nanoscale nickel, copper, and aluminum metals were reported to have catalytic activity on AP decomposition. Whereas, AP demonstrated decomposition enthalpy of 0.44 KJ/g; nanoscale transition metals offered enhanced decomposition enthalpies of 1.32 KJ/g, 1.2 KJ/g, and 0.9 KJ/g for nickel, copper, and aluminum, respectively (Cai et al. 2008; Yadav et al. 2020). Additionally, the decomposition mechanism was improved (Conkling and Mocella 2012, Yadav et al. 2020, Zarko and Gromov 2016).

This study reports on the facile fabrication of ferric oxide and nickel nanoclusters, using hydrothermal processing. Enhanced particle dispersion is obligatory to secure prospected catalytic activity (Elbasuney 2014, 2015a, b). Catalyst particles were developed and re-dispersed in acetone. Colloidal particles were integrated into AP via co-precipitation technique. Elemental mapping revealed particle dispersion to the molecular level. Thermal behavior of AP nanocomposites was evaluated using DSC and TGA. AP demonstrated total heat release of 742 J/g. Nickel NPs demonstrated decrease in endothermic phase change by 49% compared with 39% for Fe_2O_3 nanocluster. AP demonstrated total heat release of 742 J/g. Nickel offered enhanced heat output by 89% compared with 57% for ferric oxide nanocluster. The two main exothermic decomposition peaks were merged into one single peak. Additionally nickel demonstrated decrease in main decomposition temperature by 105 °C compared with 62 °C for ferric oxide NPs. Nickel nanocatalyst demonstrated decrease in AP activation energy by – 10% and – 12% using Kissinger and KAS models respectively.

Experimental

Synthesis of nanocatalysts

Fe_2O_3 was synthesized by a continuous hydrothermal reactor as a 0.05 M of ferric nitrate nonahydrate at a temperature 25 °C and pressure 240 bar with a flow rate 10 mL/min and a water as a solvent at a temperature 350 °C and pressure 240 bar with a flow rate 20 mL/min. At the intersection of the two streams inside the reactor, ferric oxide nanoparticles grew continuously (Elbasuney 2015a, b, 2017). About 1 M of nickel nitrate was added to 250 mL beaker, and the pH was adjusted at 8.5, then 10 mL of hydrazine was added drop by drop with mechanical stirring at a temperature 65 °C for 15 min. Black precipitate of nickel nanoparticles was magnetic separated.

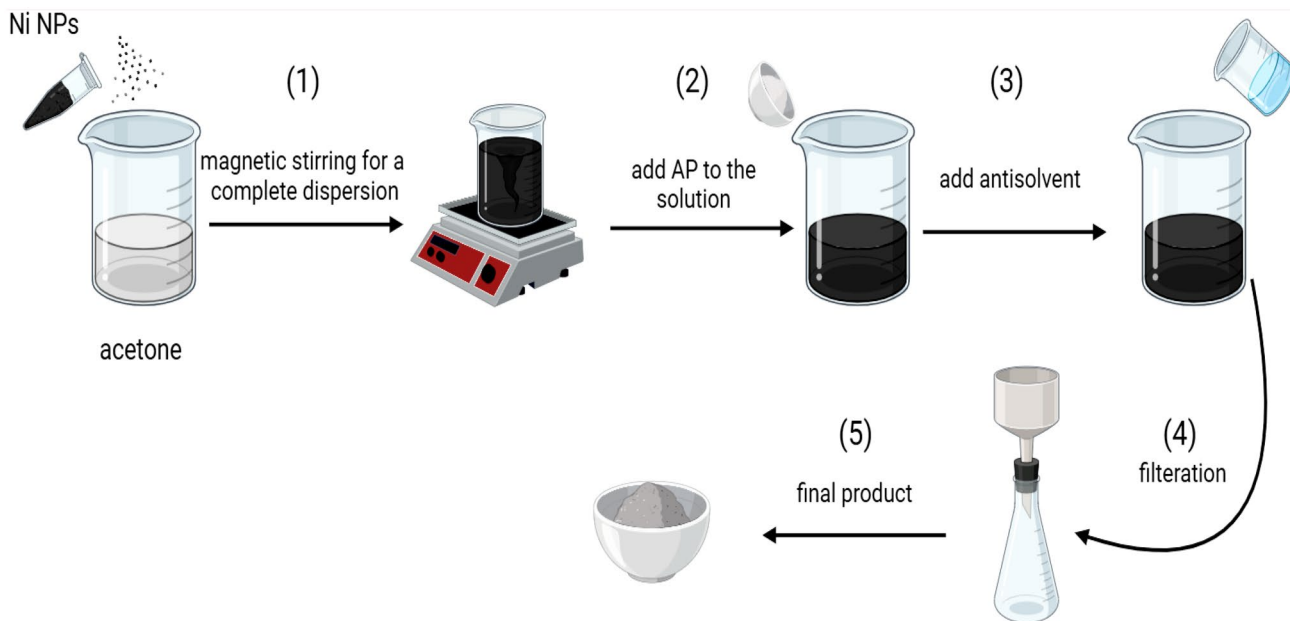


Fig. 2 Schematic diagram of Ni/AP nanocomposite development via co-precipitation method

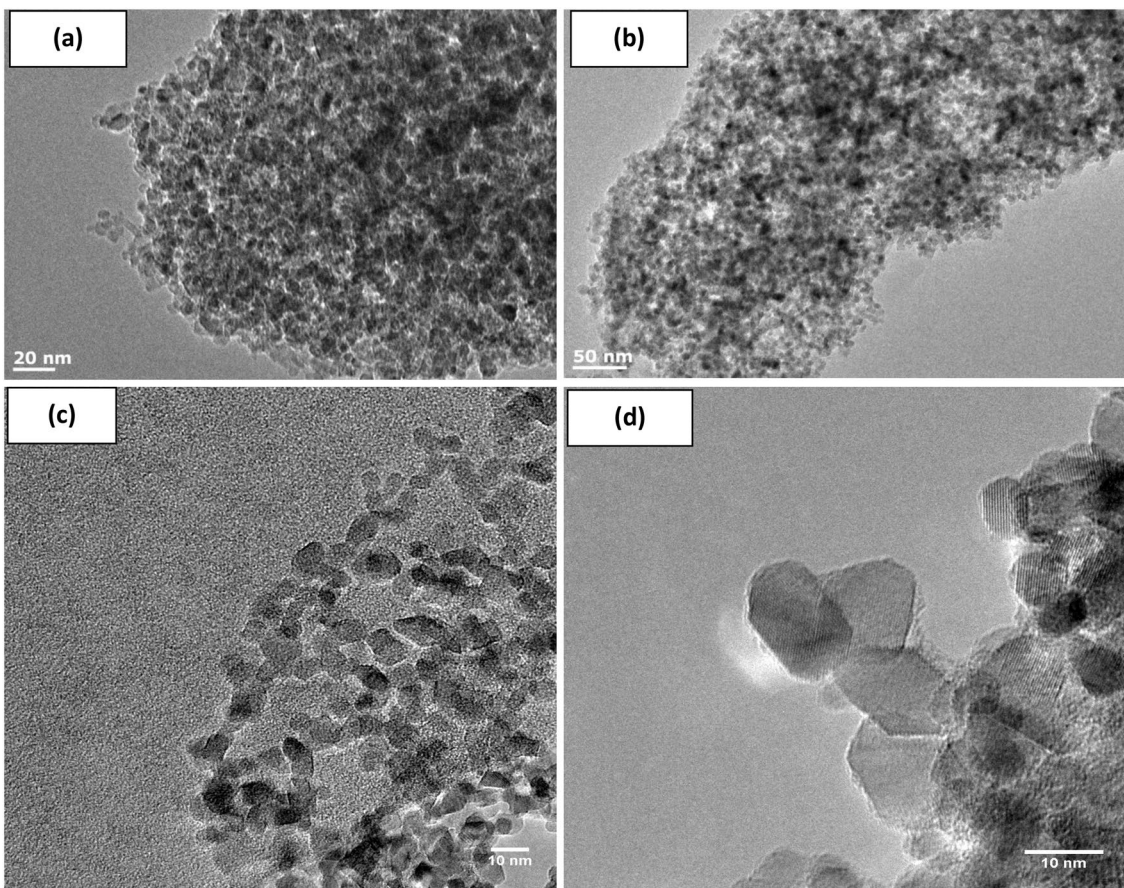


Fig. 3 TEM micrographs of synthesized ferric oxide (a, b) and nickel (c, d) nanocluster

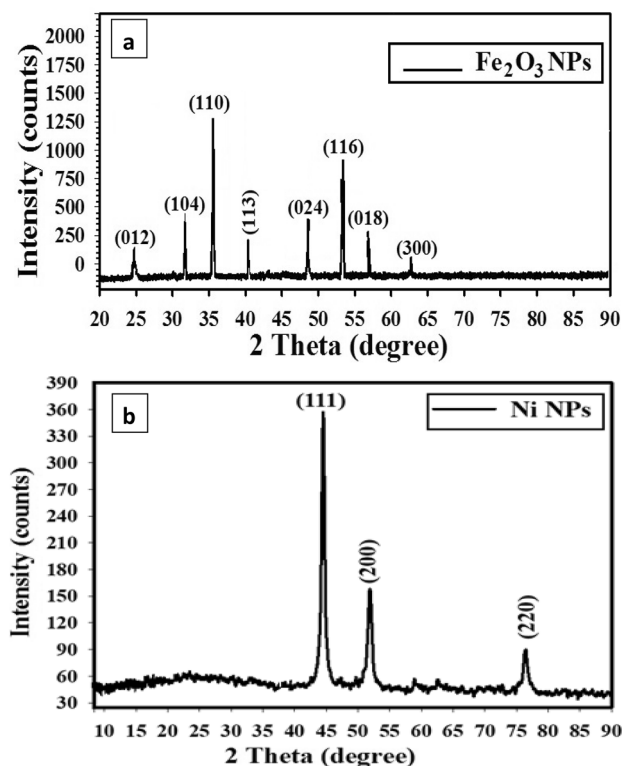


Fig. 4 XRD patterns of prepared ferric oxide NPs (a), and nickel NPs (b)

Nanocatalyst characterization

Morphology (size and shape) of ferric oxide and nickel NPs was visualized using TEM (JEM-2100 F by Joel Corporation). The crystalline structure was investigated with XRD (D8 advance by Burker Corporation). SEM (ZEISS SEM

EVO equipped with EDAX detector) was employed to assess the dispersion of NPs into AP matrix, and the corresponding elemental analysis.

Integration of nanocatalysts into AP matrix

Colloidal ferric oxide and nickel NPs were harvested from their synthesis medium and re-dispersed in acetone using ultrasonic probe homogenizer. The solvent is acetone to AP while it is dissolved Ni or Fe₂O₃ NPs dispersed under sonication, adding dichloromethane as an anti-solvent to precipitate AP (Fig. 2). Morphology of AP nanocomposite was investigated using SEM. Elemental mapping using EDAX detector was adopted to assess the catalyst dispersion into AP matrix.

Catalytic activity assessment

The potentials of developed nanocatalysts on AP thermal behavior was assessed using DSC Q20 by TA, USA. The tested sample was heated to 500 °C at 10 °C/min with a mass 1 mg, under inert gas flow (N₂ at 50 mL min⁻¹). Thermal behavior of AP nanocomposite was assessed using TGA (55 by TA, USA). The tested sample was heated to 500 °C at 10 °C with a mass 1 mg, under inert gas flow (N₂ at 50 mL min⁻¹).

Decomposition kinetics of Ni/AP nanocomposite

Decomposition kinetic study of Ni/AP nanocomposite was conducted via Kissinger and Kissinger–Akahira–Sunose (KAS) models respectively. Kinetic decomposition of Ni/AP nanocomposite was investigated using TGA at different

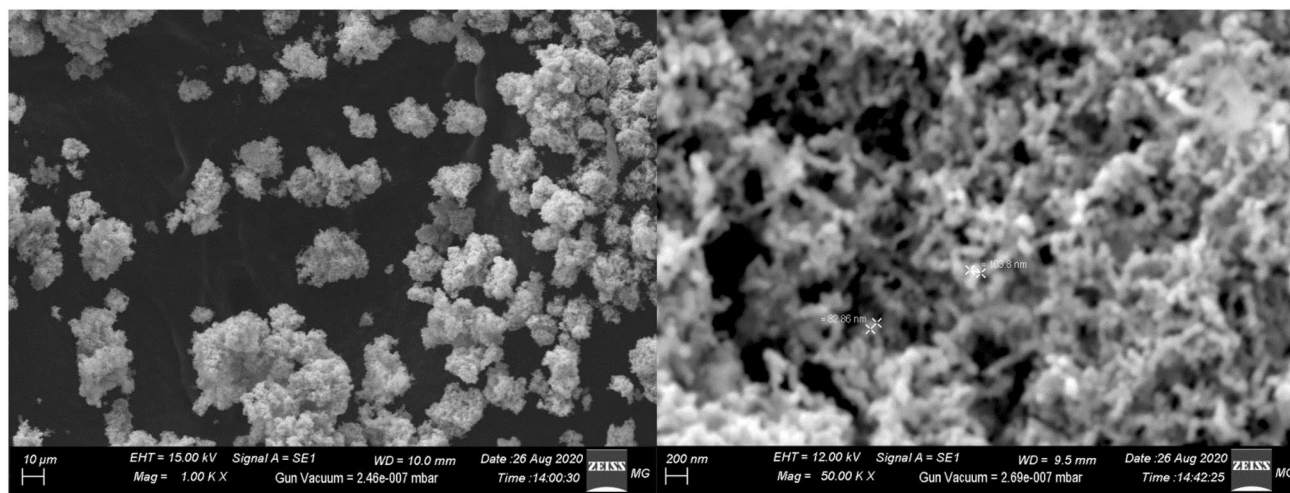


Fig. 5 SEM micrographs of dry Ni nanocluster

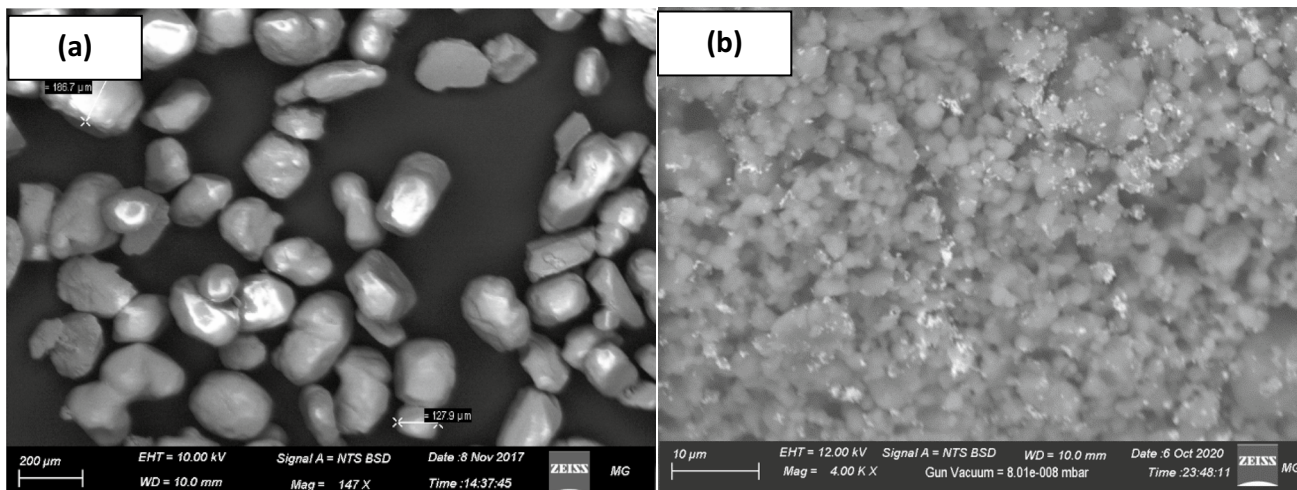


Fig. 6 SEM micrographs of starting AP (a), AP nanocomposite (b)

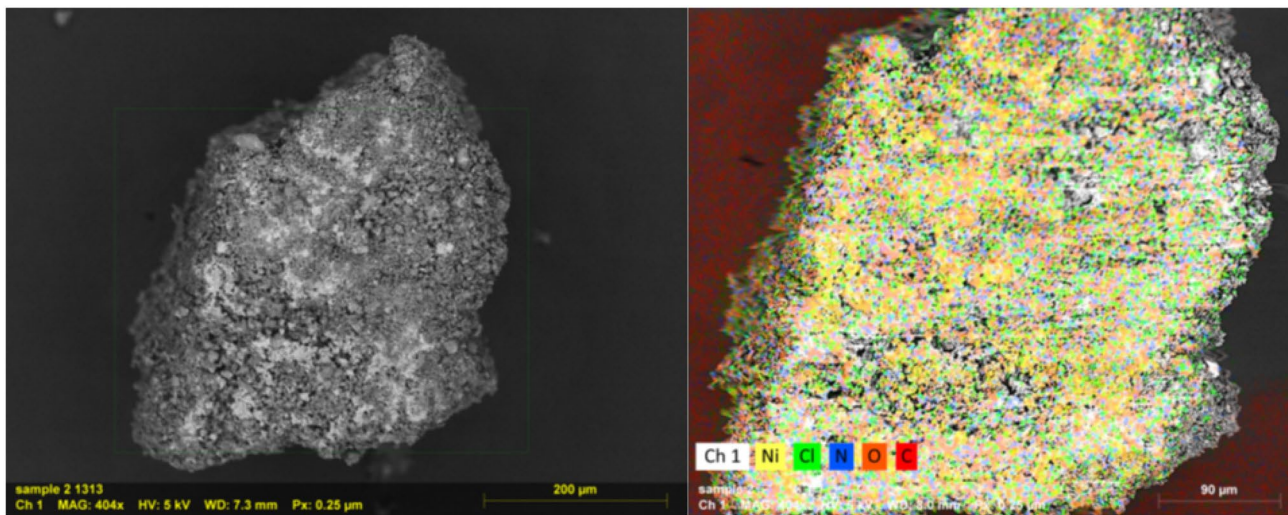


Fig. 7 Elemental mapping of Ni/AP nanocomposite using EDAX detector

Fig. 8 Impact of nanocatalyst particles on AP thermal decomposition using DSC.

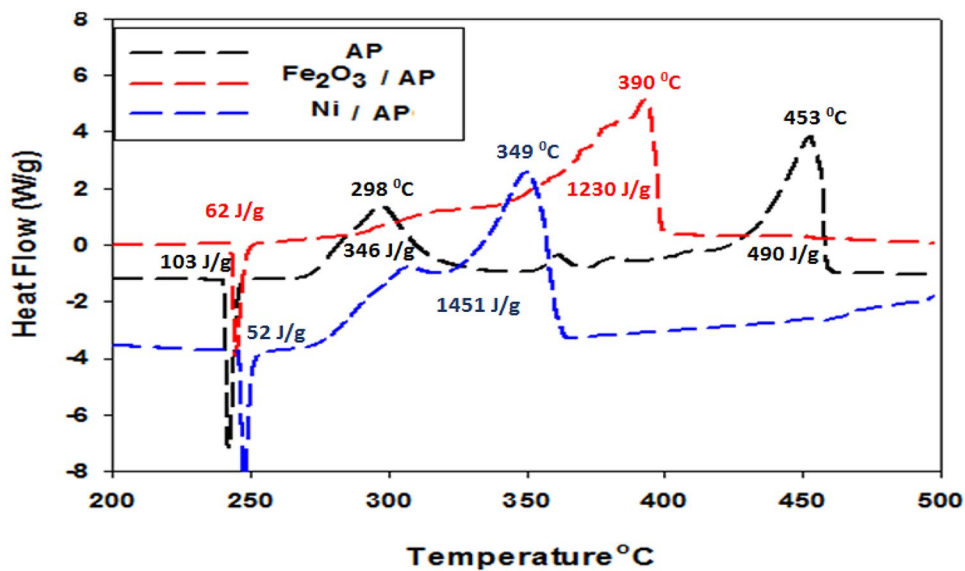
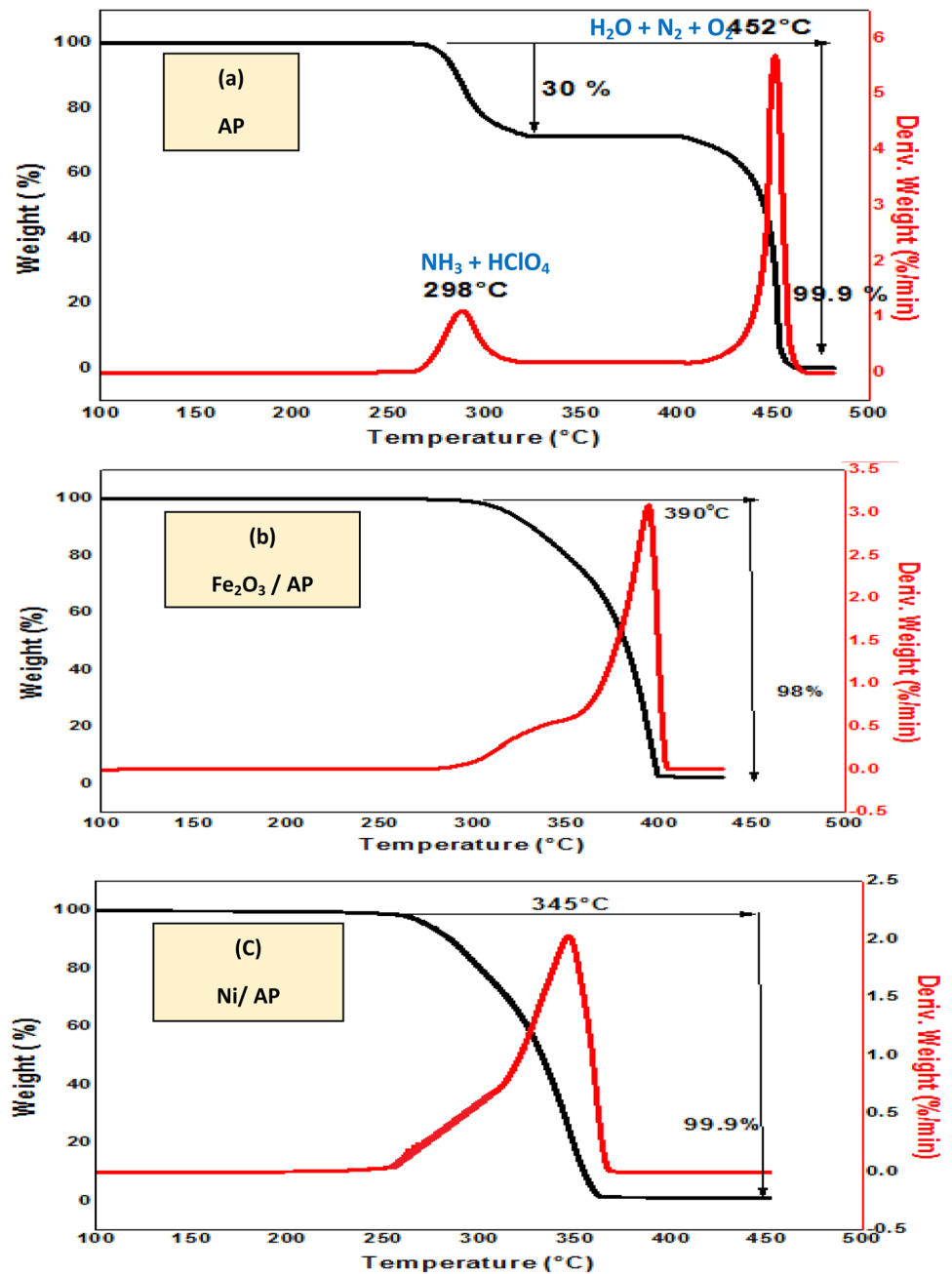


Fig. 9 Impact of nanocatalyst on AP thermal behavior using TGA, where (a) for AP, (b) for Fe₂O₃/AP, and (c) for Ni/AP



heating rates. Activation energy (E_a) of developed Ni/AP nanocomposite was evaluated from Kissinger's model (Eq. 1) (Elbasuney et al. 2021)

$$\frac{E_a}{R} = \frac{d \ln(\beta/T_p^2)}{d(1/T_p)} \quad (1)$$

Where E_a is the activation energy, β is heating rate, T is the decomposition temperature and R is universal gas constant. Evaluation of activation energy (E_a) can be accomplished by KAS model (Eq. 2) (Akahira 1971; Elbasuney et al. 2021).

To get the slope $-\frac{E_a}{R}$ from $\ln(\beta/T_p^2)$ against $(1/T_p)$

$$\ln\left(\frac{\beta_i}{T_{\alpha,i}^{1.92}}\right) = \text{Const} - 1.0008\left(\frac{E\alpha}{RT\alpha}\right) \quad (2)$$

where α is the conversion rate, T is the decomposition temperature, β heating rate, R is universal gas constant, and E is the activation energy.

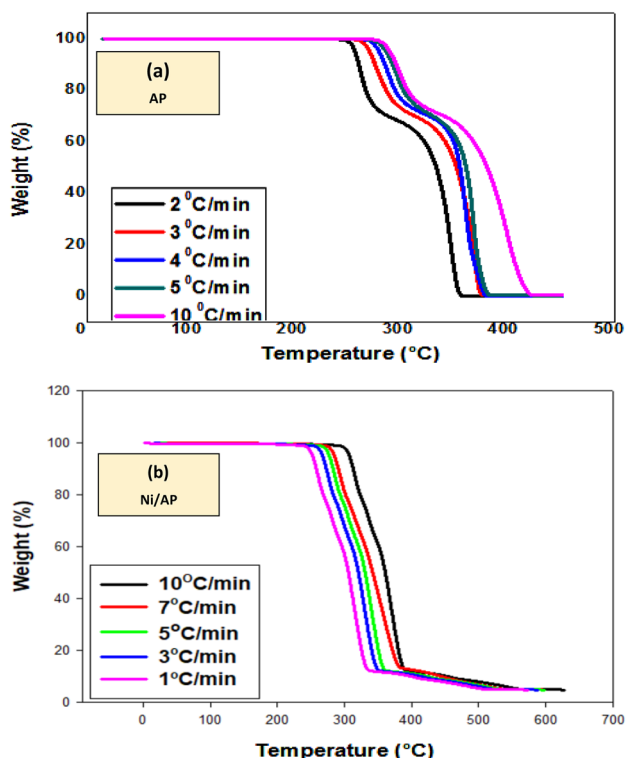


Fig. 10 TGA thermogram of AP (a), and Ni/AP nanocomposite (b)

Results and discussions

Bespoke catalyst particles can offer enhanced heat output with low activation energy. At nanoscale, superior catalytic performance could be accomplished; as high interfacial surface area and reactivity could be accomplished.

Nanocatalyst characterization

TEM micrographs demonstrated high quality mono-dispersed Fe_2O_3 nanocluster of 5 nm average particle size (Fig. 3a, and b). Mono-dispersed nickel nanocluster of 10 nm were reported from TEM micrographs (Fig. 3 and d).

XRD pattern was used to identify crystal structure and phase analysis. XRD pattern of ferric oxide nanocluster and nickel nanocluster were illustrated in Fig. 4. Figure 4 (a) show some of the distinctive peaks of ferric oxide nanocluster (JCPDS No. 33–0664). These peaks were appeared at 2θ and diffraction planes of 24.15° (012), 33.17° (104), 35.70° (110), 40.90° (113), 49.40° (024), 54.10° (116), 57.60° (018), and 62.35° (300). This matches well with the unique ferric oxide nanocrystal structure with a rhombohedral centered hexagonal phase that belonged to the space group of R3c (Hua and Gengsheng 2009, Lassoued et al. 2017, Wang et al. 2013).

Also, XRD peaks of Ni nanocluster appeared at 2θ 44.15° , 51.09° and 76.13° assigned to diffraction planes of (111), (200), and (222), respectively as presented in Fig. 4 (b). It is the characteristic XRD pattern of a face-centered cubic (fcc) phase of Ni nanocluster without any additional peaks, showing that the Ni NPs possess a single fcc phase. The broad XRD peaks were suggestive of the ultrafine nature of the prepared Ni nanocluster (Jayaseelan et al. 2014; Wang et al. 2008). XRD patterns confirmed the successful preparation of ferric oxide and nickel nanocluster. From the XRD data for both Ni and Fe_2O_3 nanocluster, we calculate the average crystallite size and was found to be 13.2 nm for Ni, and 11.1 nm for Fe_2O_3 nanocluster by applying Scherrer equation. It is necessary to compare the results of TEM with XRD data for Ni, and Fe_2O_3 nanocluster, and the results were in the same line regarding the size of the presented nanocluster after applying the Scherrer equation. The TEM results agreed well with those of XRD measurements for narrow grain size distributions with smaller mean values.

SEM micrographs of dry nickel nanocluster were investigated with SEM. SEM micrographs demonstrated fine porous aggregated material (Fig. 5). Ferric oxide nanocluster demonstrated similar tendency to aggregate with drying process (File not represented).

Characterization AP nanocomposite

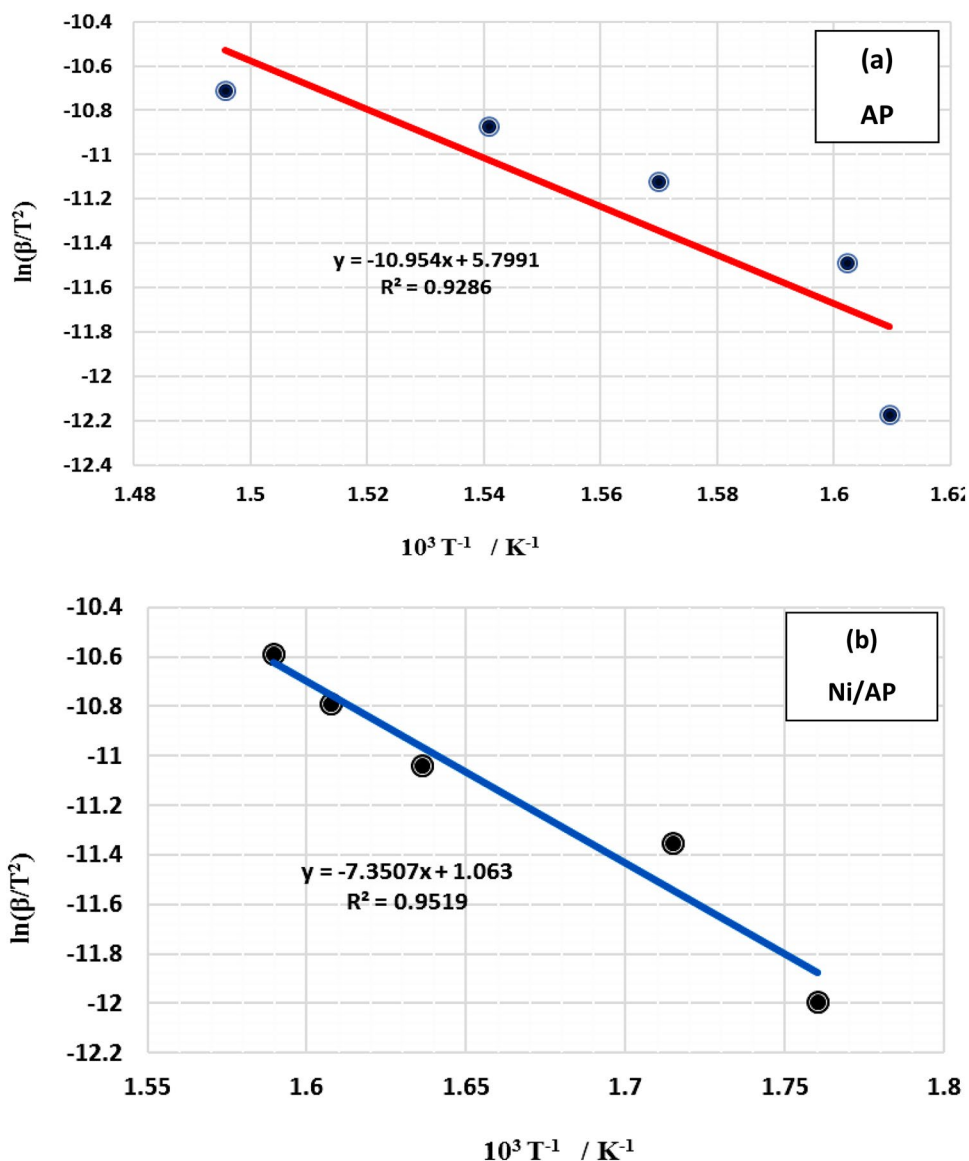
Morphology of AP nanocomposite was investigated with SEM to starting AP. Whereas starting AP demonstrated cubic particles of $150\ \mu\text{m}$ size (Fig. 6a); AP nanocomposite demonstrated ultrafine particles of $5\ \mu\text{m}$ size (Fig. 6b).

It can be concluded that the integration of colloidal particles into AP via anti-solvent technique offered uniform particles into AP matrix. Elemental mapping was performed to verify catalyst particle dispersion. SEM micrographs of AP nanocomposite revealed enhanced levels of nickel nanocluster dispersion into AP (Fig. 7). Integration of colloidal nanocatalysts into AP matrix secured uniform particle dispersion to the molecular level.

Thermal behavior of AP nanocomposite

The catalytic efficiency of nickel to ferric oxide nanocluster on AP thermal behavior was investigated using DSC. Whereas, AP demonstrated endothermic crystallographic phase change by $103\ \text{J/g}$; nickel nanocluster demonstrated decrease in endothermic crystallographic phase change by 49% compared with 39% for ferric oxide. While AP demonstrated total heat release of $742\ \text{J/g}$. Nickel nanocluster

Fig. 11 Activation energy of AP (a), and Ni/AP nanocomposite (b) using Kissinger model



offered enhanced heat output by 89% compared with 57% for ferric oxide nanocluster (Fig. 8).

The two main exothermic decomposition peaks were merged into one single peak. Additionally nickel demonstrated decrease in main decomposition temperature by 105 °C compared with 62 °C for ferric oxide NPs. The impact of catalyst nanocluster on AP thermal behavior was further evaluated using TGA. (Fig. 9a) show AP has a two decomposition temperature at 298 °C which 30% partial decomposition, and 70% complete decomposition occur at 458 °C, Adding Ni nanocluster to AP merge two exothermic peaks in one peak at 345 °C (Fig. 9c), while Fe_2O_3 show decomposition temperature at 390 °C (Fig. 9b) which is confirmed with DSC results.

Kinetic study of Ni/AP nanocomposite

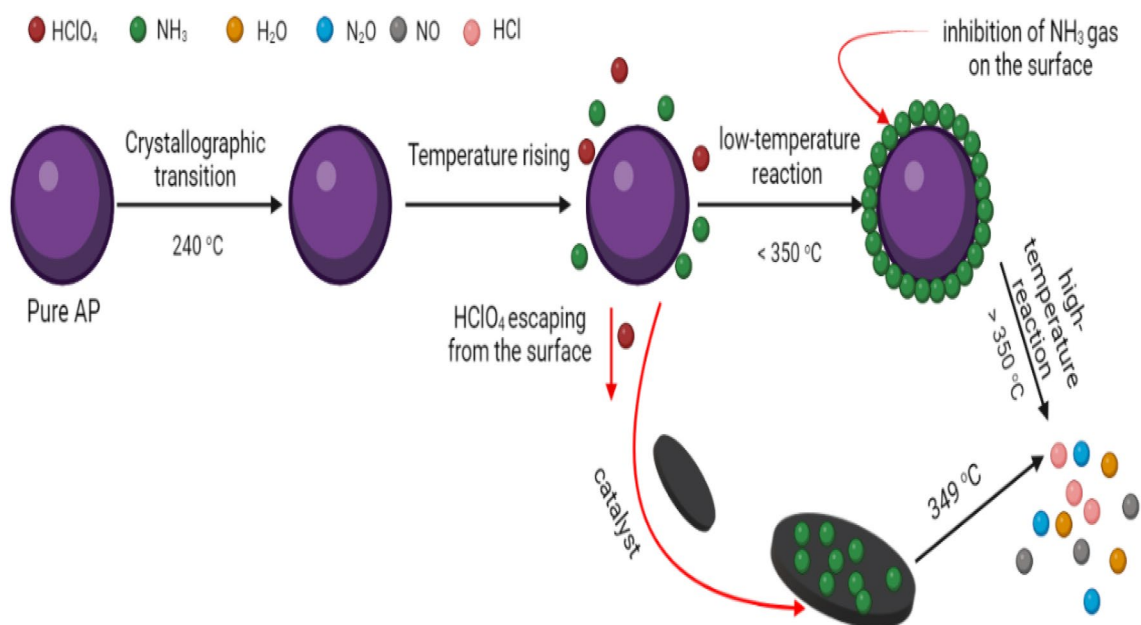
Kinetic parameters via Kissinger model

Kissinger model is based on the highest decomposition peak temperature obtained from the DTG thermogram (Fig. 10) as shown for virgin AP (Fig. 10a), and for Ni/AP nanocomposite as inhibited in Fig. 10b which matched with the previously published article (Elbasuney et al. 2021).

The activation energy of Ni/AP nanocomposite was evaluated to AP; activation energy was obtained from the slope of the straight line by plotting $\ln(\beta/T^2)$ versus $(1/T)$ at the five heating rates (Fig. 11).

Table 1 Kinetic parameters of AP and Ni/AP nanocomposite using KAS model

α reacted	Ni/AP nanocomposite			AP		
	Ea (kJ mol ⁻¹)	Log A (s ⁻¹)	r	Ea (kJ mol ⁻¹)	Log A (s ⁻¹)	r
0.05	82.6	12.7	0.972	90	15	0.982
0.10	83.7	15.3	0.983	92	17	0.993
0.15	84.3	16.8	0.986	93	13	0.987
0.20	82.1	11.8	0.989	95	14	0.989
0.25	85.6	25.7	0.990	96	17	0.992
0.30	83.1	23.3	0.982	89	15	0.992
0.35	85.4	28.2	0.983	90	16	0.988
0.40	84.7	25.2	0.994	95	14	0.995
0.45	82.6	12.9	0.986	92	13	0.996
0.50	81.5	11.6	0.996	93	14	0.998
0.55	81.4	10.5	0.986	94	15	0.996
0.60	82	12.2	0.994	95	16	0.995
0.65	81.6	11.7	0.988	92	17	0.998
0.70	83.4	23	0.998	93	18	0.998
0.75	84	25	0.999	94	19	0.999
0.80	85.3	28.1	0.998	95	14	0.998
0.85	82.6	12	0.999	941	15	0.999
0.90	85.3	28.8	0.999	94	14	0.999
Mean	83.4	18.6		93.1	15.3	

**Fig. 12** Catalytic mechanism of AP decomposition by nickel NPs.

While virgin AP demonstrated activation energy of 92.1 kJ/mol; Ni/AP nanocomposite demonstrated an activation energy of 83.7 kJ/mol. Nickel nanocatalyst can induce condensed phase reactions; that could boost

decomposition enthalpy and minimize enthalpy of endothermic phase change. This catalytic action could withstand the low activation energy.

Kinetic parameters via (KAS) model

Activation energy at different fractional conversion was determined using modified KAS model. The kinetics parameters (pre-exponential factor (A), kinetic model ($f(\alpha)$), activation energy (E_a), and regression factor (r)) of developed Ni/AP nanocomposite to starting AP were tabulated Table 1.

The mean value of the activation energies of Ni/AP nanocomposite was reported to be 83.4 kJ mol^{-1} compared with 93.1 kJ mol^{-1} for pure AP. Activation energy evaluation via KAS model was found to be in good agreement with Kissinger model. The catalytic effectiveness of nickel nanocluster was due to three principal parameters including:

- Decrease in heat required for endothermic phase change.
- Lower decomposition temperature.
- Boost heterogeneous reactions on the catalyst surface, with high heat output (Fig. 12).

Conclusion

Nickel and ferric oxide nanocluster of 10 nm, and 5 nm average particle sizes, respectively were developed via hydrothermal processing. Fabricated nanocluster were re-dispersed in organic solvent and effectively integrated into AP. Elemental mapping confirmed uniform particle dispersion into AP matrix. The catalytic efficiency of nickel was evaluated to ferric oxide nanocluster using DSC and TGA. Nickel demonstrated high catalytic efficiency to ferric oxide counterparts. Nickel offered decrease in AP endothermic phase change by 49% compared with 39% for ferric oxide. Whereas AP demonstrated total heat release of 742 J/g; nickel offered enhanced heat output by 89% compared with 57% for Fe_2O_3 nanocluster. Nickel nanocatalyst demonstrated decrease in AP activation energy by -10% and -12% using Kissinger and KAS models, respectively.

Author contributions SE: suggested the research topic, investigated the article, planned the research methodology, wrote the original draft, and participated in data representation and article revising and editing. SI: suggested the research topic, investigated the article, planned the research methodology, wrote the original draft, and participated in data representation and article revising and editing. MY: suggested the research topic, investigated the article, planned the research methodology, wrote the original draft, and participated in data representation and article revising and editing. GSE: suggested the research topic, investigated the article, planned the research methodology, wrote the original draft, and participated in data representation and article revising and editing.

Funding No external funding for this manuscript.

Data availability All data generated or analyzed during this study are included in this manuscript.

Declarations

Conflict of interest No conflict of interest to this paper.

Institutional review board statement Not applicable.

Informed consent statement Not applicable.

References

- Akahira T (1971) Trans. Joint convention of four electrical institutes. Res Rep Chiba Inst Technol 16:22–31
- Arroyo JL, Povea P, Faúndez R, Camarada MB, Cerda-Cavieles C, Abarca G, Manriquez JM, Morales-Verdejo C (2020) Influence iron-iron distance on the thermal decomposition of ammonium perchlorate. New catalysts for the highly efficient combustion of solid rocket propellant. J Organomet Chem 905:121020
- Budhwar AS, Gautam A, More PV, Pant CS, Banerjee S, Khanna PK (2018) Modified iron oxide nanoparticles as burn rate enhancer in composite solid propellants. Vacuum 156:483–491
- Cai W, Thakre P, Yang V (2008) A model of AP/HTPB composite propellant combustion in rocket-motor environments. Combust Sci Technol 180:2143–2169
- Conkling J, Mocella C (2012) Chemistry of pyrotechnics basic principles and theory. CRC, London
- Dillier CAM, Petersen ED, Petersen EL (2020) Isolating the effects of oxidizer characteristics and catalytic additives on the high-pressure exponent break of AP/HTPB-Composite propellants. In: Proceedings of the Combustion Institute
- Dubey R, Chawla M, Siril PF, Singh G (2013) Bi-metallic nanocomposites of mn with very high catalytic activity for burning rate enhancement of composite solid propellants. Thermochim acta 572:30–38
- Elbasuney S (2014) Dispersion characteristics of dry and colloidal nano-titania into epoxy resin. Powder Technol 268:158–164
- Elbasuney S (2015a) Surface engineering of layered double hydroxide (LDH) nanoparticles for polymer flame retardancy. Powder Technol 277:63–73
- Elbasuney S (2015b) Continuous hydrothermal synthesis of $\text{AlO}(\text{OH})$ nanorods as a clean flame retardant agent. Particuology 22:66–71
- Elbasuney S (2017) Sustainable steric stabilization of colloidal titania nanoparticles. Appl Surf Sci 409:438–447
- Elbasuney S (2018) Novel colloidal nanothermite particles (MnO_2/Al) for advanced highly energetic systems. J Inorg Organomet Polym Mater 28:1793–1800
- Elbasuney S, Yehia M (2019) Thermal decomposition of ammonium perchlorate catalyzed with CuO nanoparticles. Def Technol 15:868–874
- Elbasuney S, El-Sayyad GS (2020) The potentials of TiO_2 nanocatalyst on HMX thermolysis. J Mater Sci 31(17):14930–14940
- Elbasuney S, Yehia M (2020) Ferric oxide colloid: a novel nanocatalyst for solid propellants. J Inorg Organomet Polym Mater 30:706–713
- Elbasuney S, Elsaidy A, Kassem M, Tantawy H, Sadek R, Fahd A, Gobara M (2018) Super-thermite ($\text{Al}/\text{Fe}_2\text{O}_3$) fluorocarbon nanocomposite with stimulated infrared thermal signature via extended primary combustion zones for effective countermeasures of infrared seekers. J Inorg Organomet Polym Mater 28:2231–2240
- Elbasuney S, Gobara M, Yehia M (2019) Ferrite nanoparticles: synthesis, characterization, and catalytic activity evaluation for solid

- rocket propulsion systems. *J Inorg Organomet Polym Mater* 29:721–729
- Elbasuney S, Gobara M, Zaky MG, Radwan M, Maraden A, Ismael S, Elsaka E, Abd Elkodous M, El-Sayyad GS (2020) Synthesis of CuO-distributed carbon nanofiber: alternative hybrid for solid propellants. *J Mater Sci* 31:8212–8219
- Elbasuney S, Yehia M, Hamed A, Mokhtar M, Gobara M, Saleh A, Elsaka E, El-Sayyad GS (2021) Synergistic catalytic effect of thermite nanoparticles on HMX thermal decomposition. *J Inorg Organomet Polym Mater* 31(6):2293–2305
- Figueiredo PA, Brójo FM (2017) Theoretical analysis of ammonium-perchlorate based composite propellants containing small size particles of boron. *Energy Procedia* 136:202–207
- Gaete J, Arroyo JL, Norambuena Á, Abarca G, Morales-Verdejo C (2022) Mechanistic insights into the thermal decomposition of ammonium perchlorate: the role of amino-functionalized magnetic nanoparticles. *Inorg Chem* 61:1447–1455
- Hua J, Gengsheng J (2009) Hydrothermal synthesis and characterization of monodisperse α -Fe₂O₃ nanoparticles. *Mater Lett* 63:2725–2727
- Ishitha K, Ramakrishna PA (2014) Studies on the role of iron oxide and copper chromite in solid propellant combustion. *Combust Flame* 161:2717–2728
- Jain S, Gupta G, Kshirsagar DR, Khire VH, Kandasubramanian B (2019) Burning rate and other characteristics of strontium titanate (SrTiO₃) supplemented AP/HTPB/Al composite propellants. *Def Technol* 15:313–318
- Jayaseelan C, Abdul Rahuman A, Ramkumar R, Perumal P, Rajakumar G, Vishnu Kirthi A, Santhoshkumar T, Marimuthu S (2014) Effect of sub-acute exposure to nickel nanoparticles on oxidative stress and histopathological changes in Mozambique tilapia, *Oreochromis mossambicus*. *Ecotoxicol Environ Saf* 107:220–228
- Lassoued A, Dkhil B, Gadri A, Ammar S (2017) Control of the shape and size of iron oxide (α -Fe₂O₃) nanoparticles synthesized through the chemical precipitation method. *Results Phys* 7:3007–3015
- Manash A, Kumar P (2019) Comparison of burn rate and thermal decomposition of AP as oxidizer and PVC and HTPB as fuel binder based composite solid propellants. *Def Technol* 15:227–232
- Meyer R, Kohler J, Homburg A (2007) *Explosives*. WILEY, Weinheim
- Pang W-Q, DeLuca LT, Fan X-Z, Glotov OG, Wang K, Qin Z, Zhao F-Q (2020) Combustion behavior of AP/HTPB/Al composite propellant containing hydroborate iron compound. *Combust Flame* 220:157–167
- Sangtyani R, Saha HS, Kumar A, Kumar A, Gupta M, Chavan PV (2019) An alternative approach to improve burning rate characteristics and processing parameters of composite propellant. *Combust Flame* 209:357–362
- Sharma JK, Srivastava P, Singh G, Akhtar MS, Ameen S (2015) Biosynthesized NiO nanoparticles: potential catalyst for ammonium perchlorate and composite solid propellants. *Ceram Int* 41:1573–1578
- Tang D-Y, Fan Z-M, Yang G, Wang Y, Liu P-J, Yan Q-L (2020) Combustion performance of composite propellants containing core-shell Al@M(IO₃)_x metastable composites. *Combust Flame* 219:33–43
- Wang Y, Zhu J, Yang X, Lu L, Wang X (2005) Preparation of NiO nanoparticles and their catalytic activity in the thermal decomposition of ammonium perchlorate. *Thermochim acta* 437:106–109
- Wang H, Kou X, Zhang J, Li J (2008) Large scale synthesis and characterization of Ni nanoparticles by solution reduction method. *Bull Mater Sci* 31:97–100
- Wang F, Qin XF, Meng YF, Guo ZL, Yang LX, Ming YF (2013) Hydrothermal synthesis and characterization of α -Fe₂O₃ nanoparticles. *Mater Sci Semiconduct Process* 16:802–806
- Yadav N, Srivastava PK, Varma M (2020) Recent advances in catalytic combustion of AP-based composite solid propellants. *Defence Technology*
- Zarko VE, Gromov AA (2016) *Energetic nanomaterials synthesis, characterization, and application*. Elsevier, Amsterdam
- Zheng X, Li P, Zheng S, Zhang Y (2014) Thermal decomposition of ammonium perchlorate in the presence of Cu(OH)₂·2Cr(OH)₃ nanoparticles. *Powder Technol* 268:446–451

Publisher's Note Springer Nature remains neutral with regard to jurisdictional claims in published maps and institutional affiliations.

Springer Nature or its licensor (e.g. a society or other partner) holds exclusive rights to this article under a publishing agreement with the author(s) or other rightsholder(s); author self-archiving of the accepted manuscript version of this article is solely governed by the terms of such publishing agreement and applicable law.